NANO LETTERS

Letter

pubs.acs.org/NanoLett

Bidirectional Optical Sorting of Gold Nanoparticles

M. Ploschner,*[,†] T. Čižmár,[‡] M. Mazilu,[†] A. Di Falco,[†] and K. Dholakia[†]

[†]SUPA, School of Physics and Astronomy, University of St Andrews, St Andrews KY16 9SS, United Kingdom

[‡]School of Medicine, Medical and Biological Science Building, University of St Andrews, St. Andrews KY16 9TF, United Kingdom

Supporting Information

ABSTRACT: We present a generic technique allowing size-based all-optical sorting of gold nanoparticles. Optical forces acting on metallic nanoparticles are substantially enhanced when they are illuminated at a wavelength near the plasmon resonance, as determined by the particle's geometry. Exploiting these resonances, we realize sorting in a system of two counter-propagating evanescent waves, each at different wavelengths that selectively guide nanoparticles of different sizes in opposite directions. We validate this concept by demonstrating bidirectional sorting of gold nanoparticles of either 150 or 130 nm in diameter from those of 100 nm in diameter within a mixture.

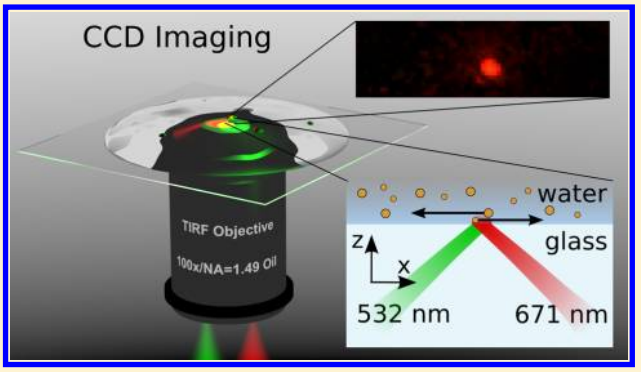

KEYWORDS: *Gold nanoparticle, optical sorting, optical manipulation, counter-propagating geometry, evanescent field, plasmon resonance*

Gold nanoparticles have unique optical and chemical properties. Their optical properties are determined by their plasmon resonances, associated with the collective excitation of conduction electrons, which in turn is dictated by the particle geometry. Further, their chemical properties allow for diverse functionalization options. For these reasons, gold nanoparticles have emerged as ideal candidates for an exceptionally wide range of biomedical applications.[1] They are commonly employed for surface-enhanced Raman spectroscopy (SERS) and as fluorescence enhancers in various applications, for example, intracellular biochemical composition imaging,[2] DNA and RNA detection,[3] and tumor targeting.[4] Additionally, they are used as mechanical carriers through cell membranes for DNA and drug delivery[5] and as localized heaters for photothermal therapy.[6] Crucially, gold nanoparticles show immense promise for multimodal biomedical applications,[7] for example, mechanical delivery with subsequent biochemical sensing and imaging. In all these cases, the physical shape and size of the gold nanoparticles dictate their performance. For example, size is a crucial parameter for the cell uptake rate of gold nanoparticles as mechanical carriers,[8,9] the intensity of a SERS signal,[10,11] the biochemical,[12] optical[13] and toxicity[14] properties of nanoparticles. It is thus necessary to tailor this parameter to a high degree of accuracy for each specific application. This results in a burgeoning need for size selective controlled separation and manipulation of gold nanoparticles in solution.

Various chemical synthesis methods[15−17] yield gold nanoparticles of different sizes within a range from 2 to 200 nm and a typical polydispersity of at least 10%. The scaling of the synthesized volume can be complicated as vigorous stirring of reducing agent and homogeneous temperature is necessary for obtaining an acceptably low level of polydispersity and the optimal conditions for this change abruptly with volume. Various postsynthetic sorting methods such as sedimentation[18] or centrifugation[19] have been developed, however their dynamic range of sorting may be limited. On the other hand, purely optical based sorting or selection methods[20−25] have the potential to sort or fractionate nanoparticles over a wide range of particle sizes in a sterile manner with exceptional sensitivity and show excellent compatibility with microfluidic environments.

Optical sorting of dielectric particles in the absence of flow has been realized by means of translating near-field evanescent wave interference patterns,[26,27] with far-field interference patterns,[28] Bessel modes,[29] and proposed within an optical conveyor belt created with a dual beam photonic crystal fiber system.[30] However, metal nanoparticles, and particularly their resonant effects, have not been appropriately considered nor exploited for any form of experimental optical sorting. To date, optical sorting realizations have mainly focused on dielectric particles or cells, largely at the micrometer size scale with only a few theoretical studies[31,32] exploring the possibility to extend the range of this powerful method to the case of plasmonic nanoparticles such as gold and silver. Since the optical forces acting on metallic nanoparticles vary significantly with particle properties such as size and composition, particularly when close

Received: December 12, 2011
Revised: March 16, 2012
Published: March 26, 2012

ACS Publications © 2012 American Chemical Society

to plasmon resonance conditions, there is an opportunity for optical sorting utilizing this behavior.

In this Letter, we present the experimental demonstration of size selective bidirectional optical sorting of gold nanoparticles using a dual wavelength counter-propagating evanescent wave geometry (Figure 1). Our technique is based on the redshift of the plasmon resonance with increasing particle size. As a result, smaller nanoparticles predominantly interact with shorter wavelengths whereas larger nanoparticles are mainly influenced by longer wavelengths (Figure 2a) (see Supporting Information B for details regarding the wavelength selection). Selecting the optimal wavelengths and power ratio between the counter-propagating beams we generate a force field within the illuminated region that guides nanoparticles of different sizes in opposite directions to one another, thus realizing sorting. The presented configuration extends optical sorting methods to the distinct case of plasmonic nanoparticles and size scales typically an order of magnitude lower than previously realized with dielectric objects.[26−30] We chose a near-field evanescent wave method for our experimental realization as it offers both the ability to sort over extended area and enables particle confinement close to an interface.[26,33]

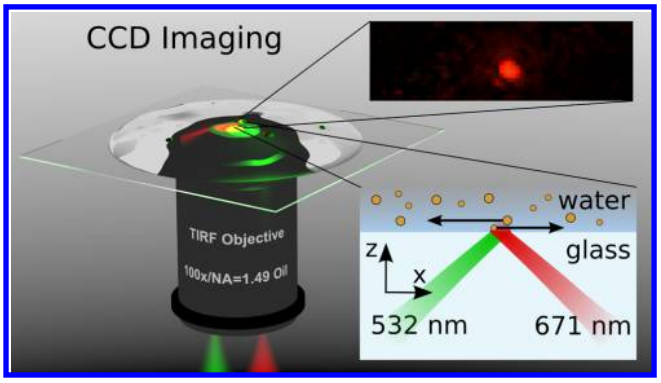

Figure 1. Two Gaussian beams with wavelengths of λ = 532 nm and λ = 671 nm, respectively, are focused to the opposite edges of the back-focal plane of a total internal reflection fluorescence (TIRF) objective (Nikon NA = 1.49, 100×). The beams propagate at the critical angle to the interface, where the counter-propagating evanescent field is generated. This both attracts the particles toward the substrate and guides them in the $\pm x$-direction. The balance of the forces from the two lasers is such that the particles of different diameter move in the opposite directions. The evanescent field scattered by particle into far-field is used for CCD imaging. The imaged particle appears red as part of the scattered field corresponding to λ = 532 nm is filtered.

The interaction of metallic nanoparticles with the evanescent waves considered here is numerically studied in Figure 2. Figure 2a shows the forces experienced by the particle as a function of its diameter for the two wavelengths selected. The difference in behavior is due to the plasmon resonance, which is highlighted in Figure 2b. The peaks in the force normalized by the geometrical cross-section give evidence of the increased coupling efficiency of the light into the nanoparticle due to the plasmon resonance. We remark that a dielectric particle on this size scale and at these wavelengths would not exhibit any resonance effect precluding their sorting using this approach.

A nanoparticle of a given size experiences a total force due to the cumulative effect of the two optical fields with a terminal velocity shown in Figure 2c. The optical force and corresponding terminal velocity were calculated for a gap of 50 nm between the particle and the interface. The corrections due to the proximity of the interface were also included.[34] Altering the intensity ratio between the beams shifts the threshold diameter for which the velocity changes sign. In our

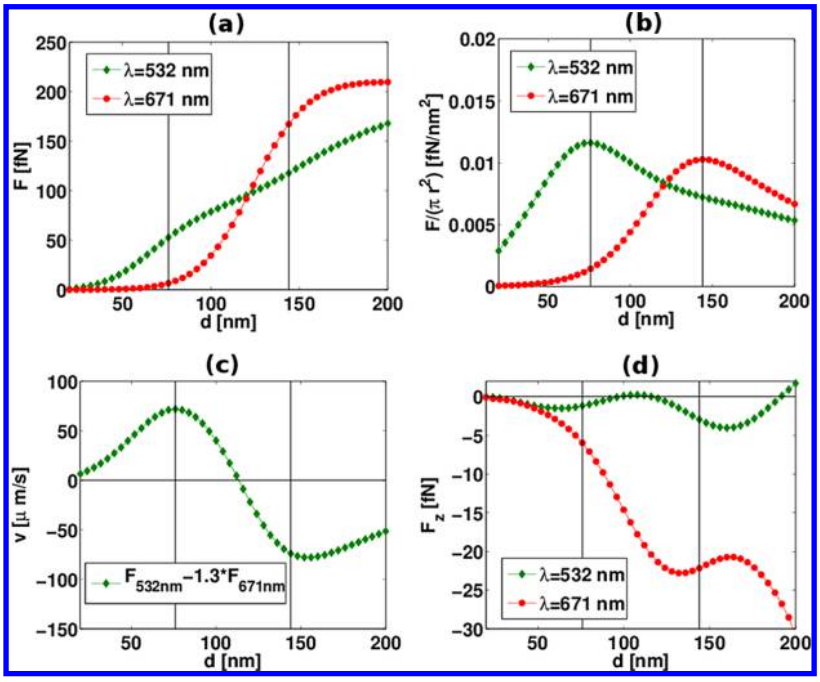

Figure 2. (a) The in-plane (x,y) optical force as a function of particle diameter calculated for a p-polarized plane-wave (incident intensity of 0.15 mW/μm^2 for both wavelengths). We considered an incident angle of θ = 62° at the glass−water interface (details of numerical simulation in Supporting Information A). (b) Interaction efficiencies as a function of nanoparticle size for the two wavelengths used. (c) Velocity of the particles in counter-propagating evanescent field with intensity I_{532} = 0.15 mW/μm^2 and I_{671} = 0.2 mW/μm^2 used in the experiment. (d) Vertical attractive forces (z-direction) acting on nanoparticles of different diameters.

dx.doi.org/10.1021/nl204378r | Nano Lett. 2012, 12, 1923−1927

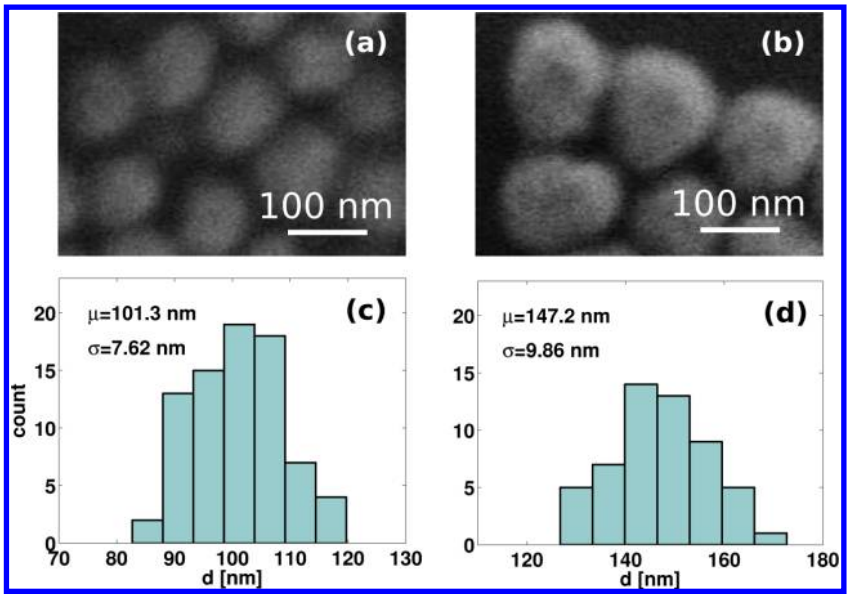

Figure 3. SEM picture of nanoparticles with nominal diameter of (a) 100 nm and (b) 150 nm. Histograms of particle diameters with mean μ and standard deviation σ values for (c) 100 nm and (d) 150 nm.

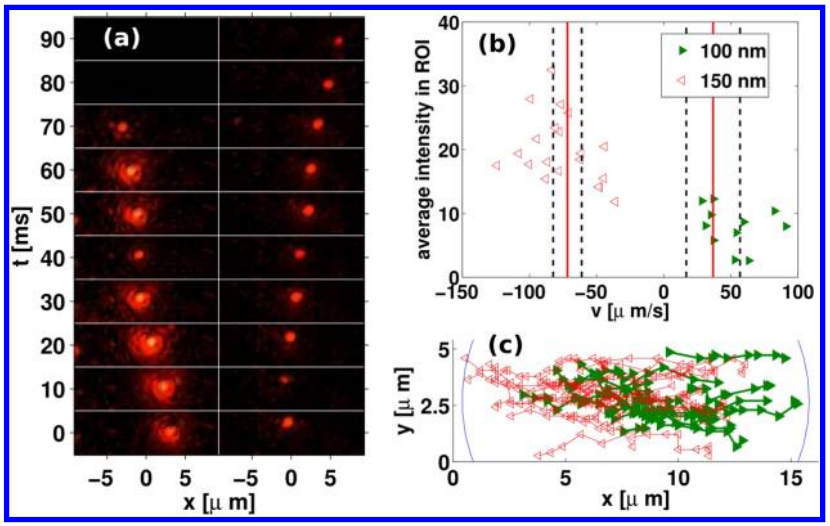

Figure 4. (a) Sequence of frames for two selected particle events. The left sequence corresponds to the larger nanoparticle (150 nm), and the right sequence shows the smaller one (100 nm). (b) The statistics shows the separation into two separate clusters with velocities being in opposite directions as expected. The vertical full red lines show predicted mean velocities for normally distributed sizes in ensembles with mean diameter of 100 and 150 nm. The black dashed lines show standard deviation of velocities for the same ensembles. The ROI is the region of interest recorded by the camera and depicted in (a). (c) The trajectories of the particles corresponding to data points in (b). The blue curve shows the waists w_0 of the incident light fields.

specific case, selecting the value of the ratio as I_{671}/I_{532} = 1.3 yields the threshold nanoparticle diameter of d = 110 nm.

The simplified experimental scheme (the detailed scheme is presented in Supporting Information F) for optical sorting is shown in Figure 1. Two diode pumped solid-state lasers (MGL-III-532−300 mW, λ = 532 nm, Laser 2000) and (MRL-III-671−300 mW, λ = 671 nm, Laser 2000) were focused to the opposite edges of the back-focal plane of a TIRF (NIKON Apo, NA = 1.49) oil immersion objective. The objective's high NA allows for incident beam angles necessary for the generation of evanescent fields and a facile incident angle control when compared to the Kretchmann prism-coupling geometry. The focusing of the beams at the back-focal plane (angular spectrum plane) ensures a very narrow wavevector distribution of the field within the sample plane. The angle of incidence of the beams is controlled by two steering mirrors positioned in a plane conjugate to the sample plane. This configuration keeps the position of the beams fixed in the sample plane while enabling a variation of the incident angle. The beam waist of each of the two beams in the sample plane is equal to 8.5 mm, which provides a sufficiently large two-dimensional region for sorting. The critical angle for both lasers is found by detecting the scattered intensity from an immobile gold nanoparticle adhered to the glass−water interface. As the intensity at the interface peaks at the critical angle, the intensity scattered to CCD is maximum for this angle. The position of the two laser spots at the interface is then exactly overlapped by recording the scattering of an immobilized particle along several vertical and horizontal lines and detecting the position of the intensity maximum and the intensity drop along the lines. The light

dx.doi.org/10.1021/nl204378r | *Nano Lett.* 2012, 12, 1923−1927

scattered from particles to CCD is also used for real-time particle identification. This method is feasible if the scattering cross-section changes significantly with particle size, which indeed we used in our subsequent diagnostics. Consequently, scattered light from the nanoparticles at λ = 671 nm provides better nanoparticle size discrimination than the recorded scattered light at λ = 532 nm (Figure S3 in Supporting Information C).

We have used a mixture of gold nanoparticles with diameter of 100 nm (CYTODIAGNOSTICS, CG-100−20, coefficient of variation CV = 0.08) and 150 nm (CG-Custom-150 nm, CV = 0.08) for experimental demonstration of the sorting method. The coefficient of variation corresponds to a relative standard deviation in particle diameter of 8 nm for the 100 nm nanoparticles and 12 nm for the 150 nm nanoparticles. This was confirmed from several images (Figure 3) from a scanning electron microscope (SEM). The mixture was prepared by combining 10 μL of each commercially available particle solution (both with concentration of nanoparticles of $\sim 6 \times 10^{-15}$ mol/mL). The mixture was subsequently diluted with deionized water in ratio 1:1. The resulting particle concentration allows for reasonable frequency of sorting events and negligible probability of interparticle interactions in the sorting experiments.

The sorting performance is presented in Figure 4. Figure 4a shows a time sequence for two typical sorting events in a mixture of gold nanoparticles using the real-time particle identification scheme. Both events are from the same video, recorded in the same region and with identical dual-wavelength illumination. As expected, the "low-intensity" scattering nanoparticle (100 nm) moves in one direction, while the "high-intensity" scattering particle (150 nm) moves in the opposite direction. Also we remark that the "high-intensity" scattering nanoparticle slows down significantly at around t = 40 ms when its intensity drops due to its diffusion away from the glass−water interface. This diffusion, together with particle size distribution, introduces a variation of particle velocity and of detected intensity in Figure 4b, where the entire series of sorting events, from the same video as the sequence of Figure 4a, is presented. There are two clearly distinguishable clusters separated both in velocity and in detected intensity. These clusters are representative of the respective nanoparticle size ensembles in the mixed solution. We note that experiments with a single size distribution do not show any degree of separation. The vertical axis in Figure 4b denotes the average intensity detected by the CCD over all the frames in the sorting experiment. The acquisition starts when the scattering intensity reaches a certain threshold and stops when the intensity drops below this threshold. The particle trajectories acquired in this way for the data points in Figure 4b are shown in Figure 4c. The trajectories show a clear overlap which excludes the possibility of observed behavior due to misaligned laser spots.

Particle diffusion in the z-direction induces a large variation in the scattering intensity detected by the CCD. Therefore, in general, the dynamic range of the CCD does not allow the simultaneous tracking of low scattering nanoparticles without saturating some of the camera pixels for the high scattering ones. This leads to a systematic bias for the high intensity events with expected intensity values for larger particles even higher than those measured in Figure 4b. Consequently, using a camera with higher dynamic range would improve the separation of clusters on intensity axis.

The experimental results are supported by theoretically calculated values of ensemble velocities shown in Figure 4b as full red lines for mean ensemble velocity and as dashed black lines for standard deviation in velocity. The average temperature increase in the vicinity of the particle due to laser excitation was estimated[35] to be 18 K, which was accounted for in velocity calculation by setting water viscosity to $\eta_{40\,^{\circ}\mathrm{C}} = 0.65 \times 10^{-3}$ Pa·s. The theoretical and experimental values are in very good agreement. The much narrower expected variation of velocity for 150 nm ensemble, compared to velocity variation for 100 nm ensemble, is due to very flat velocity profile around d = 150 nm in Figure 2c. Also notice that the occurrence of larger particles in sorting events is slightly higher, which is due to stronger gradient force, more efficient for attracting the particles toward surface (see Figure 2d).

Distinct separation of the velocity clusters in Figure 4b and the flat velocity profile in Figure 2c clearly indicate that the sorting scheme should be applicable for sorting of particles with smaller differences in sizes. Indeed, we have successfully repeated the experiment for particles of 100 and 130 nm in diameter (see Figure S4 in Supporting Information D for details). However, the increased overlap of scattering intensity clusters means that the identification technique of particles using the real-time detection scheme is not as definitive as for the case shown in Figure 4b. An improved detection scheme would overcome this limitation. Importantly, the velocity clusters have a significant velocity gap between them. The resolution limit of our method is discussed in detail in Supporting Information D.

In summary, we have demonstrated first experimental realization of size-selective optical sorting of gold nanoparticles. Our dual wavelength configuration utilized the red shift of the plasmon resonance that appears with increasing particle size, to tailor the forces acting on nanoparticles such that nanoparticles of different sizes move in opposite directions. The method, in its current implementation, allows for separation of particles with a diameter difference of 30 nm, for the nominal diameters of 100 and 130 nm. The present resolution limit stems from the limitation of the real-time detection scheme, which is hampered by non-negligible z-diffusion of the particles. Various approaches exist for reducing the z-diffusion to improve the technique such as using a weakly focused nonresonant auxiliary laser to push nanoparticles toward the glass−water interface. Alternatively, coating the substrate with nanolayer of gold or the use of a dielectric resonator[36] may significantly enhance the gradient forces attracting the nanoparticle to the surface. In the case of a gold layer, the coupling of surface plasmon polaritons into gold layer would increase both the intensity of field at the interface and the gradient force attracting the particles toward the interface.[37,38] Intriguingly, the coupling between surface plasmon polaritons within the gold layer and localized surface plasmon supported by the nanoparticle might also offer additional degrees of freedom for tailoring the sensitivity of optical force to particle size. Finally an improvement of particle confinement is also possible through the use of shaped light fields[39] or standing wave traps.[40] We believe that nanoparticle sorting by light promises an interesting new avenue exploiting the rich dynamics of the interplay between optical forces and particle resonances.

■ ASSOCIATED CONTENT

Supporting Information

Details of numerical calculation of optical forces and velocities, wavelength selection discussion, additional sorting experiments, detailed experimental scheme, and resolution limit of our method are provided. This material is available free of charge via the Internet at http://pubs.acs.org.

■ AUTHOR INFORMATION

Corresponding Author

*E-mail: mp399@st-andrews.ac.uk.

Notes

The authors declare no competing financial interest.

■ ACKNOWLEDGMENTS

We thank the U.K. Engineering and Physical Sciences Research Council for funding. K.D. is a Royal Society-Wolfson Merit Award Holder. A.D.F. is supported by an EPSRC Career Acceleration Fellowship (EP/I004602/1).

■ REFERENCES

(1) Thakor, A. S.; Jokerst, J.; Zavaleta, C.; Massoud, T. F.; Gambhir, S. S. *Nano Lett.* **2011**, *11*, 4029−4036.
(2) Ando, J.; Fujita, K.; Smith, N. I.; Kawata, S. *Nano Lett.* **2011**, *11*, 5344−5348.
(3) Cao, Y. W. C.; Jin, R. C.; Mirkin, C. A. *Science* **2002**, *297*, 1536−1540.
(4) Qian, X.; Peng, X.-H.; Ansari, D. O.; Yin-Goen, Q.; Chen, G. Z.; Shin, D. M.; Yang, L.; Young, A. N.; Wang, M. D.; Nie, S. *Nat. Biotechnol.* **2008**, *26*, 83−90.
(5) Paciotti, G. F.; Myer, L.; Weinreich, D.; Goia, D.; Pavel, N.; McLaughlin, R. E.; Tamarkin, L. *Drug Delivery* **2004**, *11*, 169−183.
(6) Gobin, A. M.; Lee, M. H.; Halas, N. J.; James, W. D.; Drezek, R. A.; West, J. L. *Nano Lett.* **2007**, *7*, 1929−1934.
(7) Choi, J.-s.; Jun, Y.-w.; Yeon, S.-I.; Kim, H. C.; Shin, J.-S.; Cheon, J. *J. Am. Chem. Soc.* **2006**, *128*, 15982−15983.
(8) Chithrani, B. D.; Ghazani, A. A.; Chan, W. C. W. *Nano Lett.* **2006**, *6*, 662−668.
(9) Chithrani, B. D.; Chan, W. C. W. *Nano Lett.* **2007**, *7*, 1542−1550.
(10) Jain, P. K.; Lee, K. S.; El-Sayed, I. H.; El-Sayed, M. A. *J. Phys. Chem. B* **2006**, *110*, 7238−7248.
(11) Kern, A. M.; Martin, O. J. F. *Nano Lett.* **2011**, *11*, 482−487.
(12) Jiang, W.; Kim, B. Y. S.; Rutka, J. T.; Chan, W. C. W. *Nat. Nanotechnol.* **2008**, *3*, 145−150.
(13) Kelly, K. L.; Coronado, E.; Zhao, L. L.; Schatz, G. C. *J. Phys. Chem. B* **2003**, *107*, 668−677.
(14) Pan, Y.; Neuss, S.; Leifert, A.; Fischler, M.; Wen, F.; Simon, U.; Schmid, G.; Brandau, W.; Jahnen-Dechent, W. *Small* **2007**, *3*, 1941−1949.
(15) Kimling, J.; Maier, M.; Okenve, B.; Kotaidis, V.; Ballot, H.; Plech, A. *J. Phys. Chem. B* **2006**, *110*, 15700−15707.
(16) Frens, G. *Nature (London), Phys. Sci.* **1973**, *241*, 20−22.
(17) Perrault, S. D.; Chan, W. C. W. *J. Am. Chem. Soc.* **2009**, *131*, 17042−17043.
(18) Contado, C.; Argazzi, R. *J. Chromatogr. A* **2009**, *1216*, 9088−9098.
(19) Novak, J. P.; Nickerson, C.; Franzen, S.; Feldheim, D. L. *Anal. Chem.* **2001**, *73*, 5758−5761.
(20) Kaneta, T.; Ishidzu, Y.; Mishima, N.; Imasaka, T. *Anal. Chem.* **1997**, *69*, 2701−2710.
(21) Pelton, M.; Ladavac, K.; Grier, D. G. *Phys. Rev. E* **2004**, *70*, 031108.
(22) Xiao, K.; Grier, D. G. *Phys. Rev. Lett.* **2010**, *104*, 028302.
(23) MacDonald, M. P.; Spalding, G. C.; Dholakia, K. *Nature* **2003**, *426*, 421−424.
(24) Jonas, A.; Zemanek, P. *Electrophoresis* **2008**, *29*, 4813−4851.
(25) Marchington, R. F.; Mazilu, M.; Kuriakose, S.; Garces-Chavez, V.; Reece, P. J.; Krauss, T. F.; Gu, M.; Dholakia, K. *Opt. Express* **2008**, *16*, 3712−3726.
(26) Cizmar, T.; Siler, M.; Sery, M.; Zemanek, P.; Garces-Chavez, V.; Dholakia, K. *Phys. Rev. B* **2006**, *74*, 035105.
(27) Ricardez-Vargas, I.; Rodriguez-Montero, P.; Ramos-Garcia, R.; Volke-Sepulveda, K. *Appl. Phys. Lett.* **2006**, *88*, 121116.
(28) Jakl, P.; Cizmar, T.; Sery, M.; Zemanek, P. *Appl. Phys. Lett.* **2008**, *92*, 161110.
(29) Paterson, L.; Papagiakoumou, E.; Milne, G.; Garces-Chavez, V.; Tatarkova, S. A.; Sibbett, W.; Gunn-Moore, F. J.; Bryant, P. E.; Riches, A. C.; Dholakia, K. *Appl. Phys. Lett.* **2005**, *87*, 123901.
(30) Gherardi, D. M.; Carruthers, A. E.; Cizmar, T.; Wright, E. M.; Dholakia, K. *Appl. Phys. Lett.* **2008**, *93*, 041110.
(31) Zelenina, A. S.; Quidant, R.; Badenes, G.; Nieto-Vesperinas, M. *Opt. Lett.* **2006**, *31*, 2054−2056.
(32) Quidant, R.; Zelenina, S.; Nieto-Vesperinas, M. *Appl. Phys. A* **2007**, *89*, 233−239.
(33) Kawata, S.; Sugiura, T. *Opt. Lett.* **1992**, *17*, 772−774.
(34) Leach, J.; Mushfique, H.; Keen, S.; Di Leonardo, R.; Ruocco, G.; Cooper, J. M.; Padgett, M. J. *Phys. Rev. E* **2009**, *79*, 026301.
(35) Baffou, G.; Quidant, R.; Girard, C. *Appl. Phys. Lett.* **2009**, *94*, 153109.
(36) Reece, P. J.; Garces-Chavez, V.; Dholakia, K. *Appl. Phys. Lett.* **2006**, *88*, 221116.
(37) Wang, K.; Schonbrun, E.; Steinvurzel, P.; Crozier, K. B. *Nano Lett.* **2010**, *10*, 3506−3511.
(38) Garces-Chavez, V.; Quidant, R.; Reece, P. J.; Badenes, G.; Torner, L.; Dholakia, K. *Phys. Rev. B* **2006**, *73*, 085417.
(39) Ploschner, M.; Mazilu, M.; Cizmar, T.; Dholakia, K. *Opt. Express* **2011**, *19*, 13922−13933.
(40) Demergis, V.; Florin, E.-L. *Opt. Express* **2011**, *19*, 20833−20848.